Evolution of a spherical hydrate-free inclusion in a porous matrix filled with methane hydrate

Kirill Tsiberkin,[1,*] Dmitry V. Lyubimov,[1] Tatyana P. Lyubimova,[2] and Oleg Zikanov[3]
[1]*Department of Theoretical Physics, Perm State University, Bukirev 15, 614990 Perm, Russia*
[2]*Institute of Continuous Media Mechanics UB RAS, 614013 Perm, Russia*
[3]*Department of Mechanical Engineering, University of Michigan–Dearborn, Dearborn, Michigan 48128-1491, USA*
(Received 7 September 2013; revised manuscript received 30 December 2013; published 13 February 2014)

The behavior of a small isolated hydrate-free inclusion (a gas bubble) within a porous matrix filled with methane hydrate and either water or methane gas is analyzed. Simplifying assumptions of spherical symmetry, an infinite uniform porous medium, and negligible effects of background temperature and pressure variations focus the investigation on the features of the dynamics of a single bubble determined by a phase transition. Two solutions are presented: an exact solution of the Stefan problem obtained when the effects of gas and water flow are neglected, and a numerical solution of the full problem. The solutions are in good agreement with each other and with known asymptotic dependencies, confirming that the effects of inertia and convection transport can be neglected in the case of small inclusions. It is found that, after an initial adjustment, the radius of any small bubble decreases with time following a self-similar solution of the Stefan problem. The lifetime of a bubble is evaluated as a function of initial radius and the system's physical parameters. Possible effects of such inclusions on the filtration of methane to the surface and other aspects of the dynamics of hydrate-bearing deposits are discussed.

DOI: 10.1103/PhysRevE.89.023008 PACS number(s): 44.30.+v, 44.35.+c, 47.56.+r, 64.70.D−

I. INTRODUCTION

Methane hydrate is an icelike compound in which molecules of methane are contained in a lattice formed by water molecules [1,2]. The compound is thermodynamically stable at low temperature and high pressure. The hydrates occur as natural deposits as confirmed by drilling and indirect (primarily sonic reflection) evidence. The observational data, while far from forming a complete picture, indicate that the deposits are vast, with the total carbon content certainly exceeding the cumulative content of the other fossil hydrocarbons combined [3].

The thermodynamic stability requirements limit the existence of methane hydrate to a relatively deep and narrow layer [1,2]. Underneath the layer, where temperature increases following the geothermal gradient, there often exists a sediment layer saturated with free methane gas.

Apart from their potential as a new source of fossil fuel, the current interest in natural hydrates is due to their possible role as an agent of climate change [4]. It has been hypothesized that an increase of surface temperature may lead to the dissociation of hydrates and the release of methane into the atmosphere, and with the large greenhouse capacity of methane, it may create a positive feedback loop accelerating temperature growth [5]. Estimates based on the typical times of diffusion of heat and gas through sediments (see, e.g., [4,6]), while not entirely conclusive, indicate that such a scenario is unlikely to be realized as a major component of global warming in a historically short time. The reason is that the typical time of propagation of surface temperature perturbation to major hydrate deposits and the time of filtration of methane to the surface are long: thousands of years. Still, we cannot exclude the possibility of a significant negative impact of hydrates, either in the case of shallower Arctic deposits [7] or, as we will discuss below in this paper, due to the transport mechanisms that are more potent than mere diffusion.

To assess the response of natural hydrates to global warming, as well as to develop methods of methane extraction for fuel, it is essential to understand all possible modes of filtration of methane through the hydrate-saturated porous medium. One such mode is associated with the formation of small hydrate-free inclusions within deposits saturated by hydrates, which are thermodynamically stable but close to instability. Such inclusions may form near boundaries of an extraction well or within a hydrate layer due to local pressure or temperature variations. They may also appear as a result of excursions of warm free gas and water from the underlying gas-saturated layer (see, e.g., [8]).

In the rest of the paper, the term "bubble" is used for such an inclusion. One should not confuse it with a true bubble, which is an interior of a gas-liquid interface. In our study, the term identifies a small isolated domain within the hydrate-bearing deposits in which the hydrates are absent, so the pores are filled with a gas-water mixture. The pores of the surrounding deposits contain thermodynamically stable hydrates and either excess gas or excess water. The excess gas situation is commonly observed in permafrost deposits, while the excess water case is typical for sea-shelf systems.

The influence of hydrate-free inclusions (the "bubbles") on the evolution of hydrate-bearing sediments is poorly understood. The following significant mechanisms can be predicted on the basis of general physical reasoning. First and probably foremost, if the bubbles survive for a sufficiently long time, their upward motion driven by the buoyancy force may significantly increase, perhaps manyfold, the rate of filtration of methane to the surface. Should this be true, the estimates based on the assumption of purely diffusive transport [4,6] would gravely underestimate the time of reaction of hydrate deposits to an increase of surface temperature. The models used to evaluate methane extraction techniques would also be significantly affected.

*kbtsiberkin@psu.ru

Apart from the direct contribution into the upward transport, the presence of a large number of bubbles is likely to affect the dynamics of hydrate-bearing sediments in other ways. An important aspect is the increase of the average permeability leading to stronger gas and water flows and, thus, to stronger convection heat and mass transfer. Also important and very interesting for future studies is the possibility that a large number of bubbles may cause a global morphological instability of surrounding deposits, in which accelerating local dissociation of hydrates leads to the formation of large hydrate-free pockets, which, in turn, may deform into vertical chimney-like hydrate-free channels serving as effective conduits of methane to the surface. This scenario, while yet unexplored, does not seem unrealistic, especially if we assume the situation of hydrates close to thermodynamic instability, which is routinely observed in natural deposits.

At present, all the above-mentioned effects and mechanisms are purely hypothetical. Neither observations nor theoretical studies provide sufficient material to confirm or disprove their existence. A critical missing element, upon which much of the future work will depend, is an accurate estimate of the lifetime of a single hydrate-free inclusion. This paper presents an attempt to obtain such an estimate.

We analyze the bubble's dynamics and lifetime using a simplifying model focused on the effect of phase transition and heat transfer. The model is applicable in the case of a small (few cm) bubble. The problem is solved following two approaches. In one, a numerical solution is found for the full model, in which flows of methane gas and liquid water are included. In the other, we follow the estimates of flow velocities in a poorly permeable medium, which indicate that convection heat transfer can be neglected in comparison with conduction heat transfer. The problem is reduced to a spherically symmetric Stefan problem, for which we find a full analytical solution.

The paper is organized as follows. After presenting the model and numerical method in Sec. II, we state the Stefan problem and describe its analytical solution in Sec. III. Results of numerical solution of the full problem are presented and compared with the analytical results in Sec. IV. Assessment of the possibility of a bubble floating-up through the hydrate deposit is provided in Sec. V, while Sec. VI contains concluding remarks.

II. PHYSICAL MODEL, GOVERNING EQUATIONS, AND NUMERICAL METHOD

We consider a boundless porous matrix of uniform properties with pores filled by methane hydrates and either water (excessive water situation) or methane gas (excessive gas situation). The effects of geothermal temperature gradient and background pressure variation are neglected because we consider phenomena within a small area (a few m), and temperature and pressure do not change significantly at this scale. The porous medium is assumed to be at temperature T and pressure P corresponding to hydrates, which are thermodynamically stable, but close to the equilibrium curve (the curve separating stability and instability regions of the phase diagram). We use the common approximation of the

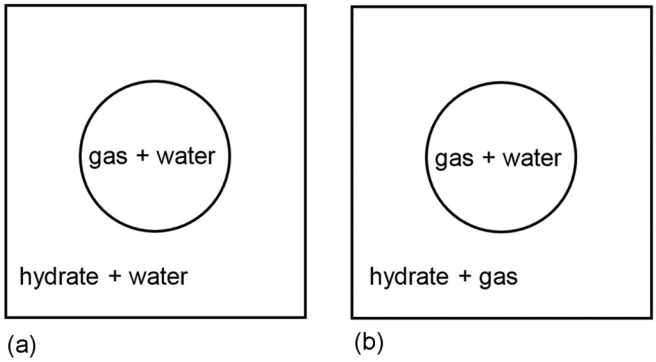

FIG. 1. Structure of a hydrate-free bubble within a hydrate-bearing porous medium in the cases of excess water (a) and excess gas (b).

curve from [9]

$$P_{\mathrm{eq}}(T_{\mathrm{eq}}) = \Pi \exp\left(A' + \frac{B'}{T_{\mathrm{eq}}}\right), \quad \Pi = 10^3 \ \mathrm{Pa},$$
$$A' = 38.98, \quad B' = -8533.8 \ \mathrm{K}. \tag{1}$$

The approximation can be applied for temperatures from 0 to 25 °C [9], which is close to the typical values of temperature in hydrate-bearing sediments [1].

A small spherical hydrate-free inclusion (a bubble) of radius R_0 exists at the initial moment within the matrix, as shown in Fig. 1. Temperature and pressure within the bubble are close to those in the surrounding matrix, but shifted via an increase of temperature or a decrease of pressure so that they are either on the equilibrium curve given by (1) or correspond to weak thermodynamic instability of hydrates.

We note that the assumed spherical shape is a simplification of the real situation, where the capillary effects and other mechanisms acting during the bubble's nucleation and growth are expected to lead to complex three-dimensional shapes. Our assumption is justified as the one giving a starting point suitable for the first study of the problem. It renders the problem easily treatable and allows us to focus on the critically important mechanism of phase transition. More realistic complex shapes of the bubble are left for exploration in future studies.

No continuing heat supply or depressurization is assumed within the bubble, so we have to expect the formation of hydrates on its boundary, and, since the thermodynamically stable surrounding matrix is assumed infinite, the gradual decrease of the bubble's radius and, eventually, its disappearance. Since the reaction of hydrate formation is exothermic, the process is controlled by transport of heat into the surrounding matrix.

We analyze the bubble's dynamics in the framework of the model that takes into account the phase transition and accompanying heat and mass transfer processes. As will be discussed in detail later, the phase transition is limited to a narrow layer between the hydrate-free and hydrate-filled domains, which we will model as an interface.

Several other simplifying assumptions are made in the model. The resistance of a porous matrix to flows of gas and water is described by the Darcy law [10]. Capillary pressure between water and gas, the solubility of gas in water, and evaporation of water into gas are not taken into account.

The solid porous matrix is assumed to be nondeformable and having constant and uniform properties, such as porosity, permeability, specific heat, and thermal conductivity. Due to the dominant contribution of the matrix, its volume-averaged specific heat and conductivity are used as cumulative specific heat and conductivity in the entire domain of analysis [11].

Bubbles of small size (few cm) are considered. In addition to rendering the background temperature and pressure gradients unimportant, this allows us to neglect the natural convection effect. This is easy to see using the evaluation of the Rayleigh number based on the bubble size [10]:

$$\mathrm{Ra} = \frac{\rho g \beta k_0 L \Delta T}{\eta \chi}, \tag{2}$$

where ρ, η, β are the fluid density, dynamic viscosity, and thermal volume expansion coefficient, k_0 is the matrix permeability, χ is the thermal conductivity, L is the characteristic linear scale of the system (about the bubble's size), and ΔT is the characteristic temperature difference. The resulting $\mathrm{Ra} \sim 10^{-6}$ is much lower than the critical number for the onset of natural convection. The effect of gravity is, thus, completely disregarded in our formulation.

Due to its much higher viscosity, the velocity of water is much lower than the velocity of gas in our system. Nevertheless, the water flow should be taken into account because of the higher heat capacity of water and the resulting possibility of a significant convective contribution into heat transfer. At the same time, changes of water saturation due to the flow are small. We can assume, as an approximation, that the saturation S_w remains constant outside the hydrate dissociation layer.

The ideal gas equation is applied to gaseous methane. This is justified since the typical temperature of the system is much higher than the methane critical point temperature. As an approximation, we apply the ideal gas equation to describe the relation between pressure, temperature, and gas density in the entire solution domain, both in hydrate-free and hydrate-filled zones. The applicability of the model is evident in systems with excess gas. In the case of systems with excess water, we use the model under the assumption that some small amount of free gases remains within the hydrate zone.

Finally, the model assumes the existence of separate hydrate-saturated and hydrate-free zones. As we will describe shortly, the interface between the zones is described by special boundary conditions, and we assume that there is no phase transition outside the interface.

With the approximations just described, the governing transport equations are

$$m_s \frac{\partial (1 - S_w - S_h)\rho_g}{\partial t} + \nabla \cdot \rho_g \boldsymbol{v}_g = \mathbf{0}, \tag{3}$$

$$\langle \rho C \rangle_s \frac{\partial T}{\partial t} + (\rho_g C_g \boldsymbol{v}_g + \rho_w C_w \boldsymbol{v}_w) \cdot \nabla T = \langle \kappa \rangle_s \nabla^2 T, \tag{4}$$

$$\boldsymbol{v}_g = -\frac{k_0 F_g(S_w, S_h)}{\eta_g} \nabla P, \tag{5}$$

$$\boldsymbol{v}_w = -\frac{k_0 F_w(S_w, S_h)}{\eta_w} \nabla P, \tag{6}$$

$$P = \rho_g R_m T, \tag{7}$$

TABLE I. Physical parameters used in the numerical model.

m_s	0.25	k_0	1.00×10^{-14} m^2
$\langle \rho C \rangle_s$	2.50×10^6 J/m^3 K	$\langle \kappa \rangle_s$	1.50 W/m K
R_m	5.20×10^2 J/kg K	L_h	5.00×10^5 J/kg
C_g	1.56×10^3 J/kg K	C_w	4.20×10^3 J/kg K
η_g	1.80×10^{-5} Pa s	η_w	1.80×10^{-3} Pa s
ρ_w	1.00×10^3 kg/m^3	ρ_h	9.00×10^2 kg/m^3
ρ_{g0}	1.16×10^2 kg/m^3	ρ_{w0}	7.84×10^2 kg/m^3

where m_s is matrix porosity, $\langle \rho C \rangle_s$ and $\langle \kappa \rangle_s$ are averaged specific heat and thermal conductivity, which we define and approximate as in Ref. [11],

$$\begin{aligned} \langle \rho C \rangle_s &= m_s[(1 - S_w - S_h)\rho_g C_g + S_w \rho_w C_w \\ &\quad + S_h \rho_h C_h] + (1 - m_s)\rho_s C_s \approx \rho_s C_s, \\ \langle \kappa \rangle_s &= m_s[(1 - S_w - S_h)\kappa_g + S_w \kappa_w + S_h \kappa_h] \\ &\quad + (1 - m_s)\kappa_s \approx \kappa_s, \end{aligned}$$

S and F are phase saturation and relative permeability, ρ, η, and $\boldsymbol{v}$ are density, dynamic viscosity, and velocity, and T and P are absolute temperature and pore pressure. Indices s, h, w, and g denote the characteristics of specific phases: solid matrix, hydrate, water, and gas. R_m is the methane gas constant.

Equations (3)–(7) form the system for the gas density ρ_g, temperature T, pressure P, and velocities $\boldsymbol{v}_g$ and $\boldsymbol{v}_w$ as unknown variables. The physical properties are constant and have the values listed in Table I. The hydrate saturation S_h is equal to a prescribed constant in the hydrate-filled area and to zero within the hydrate-free bubble. The water saturation is also given by two constants, one for each area. Outside the bubble, $S_w = 0$ in the system with excess gas or given by a nonzero constant in the system with excess water. Within the bubble, S_w is equal to a constant computed so as to maintain water balance at hydrate dissociation at the interface:

$$\rho_w S_w|_{\mathrm{in}} = \rho_w S_w|_{\mathrm{out}} + \rho_{0w} S_h|_{\mathrm{out}}, \tag{8}$$

where the indices "in" and "out" refer to fields inside and outside of the bubble, and ρ_{w0} is the mass fraction of water in hydrate composition calculated in terms of density.

The relative permeability functions F are approximated by linear relations

$$F_g(S_w, S_h) = 1 - S_w - S_h, \quad F_w(S_w, S_h) = S_w, \tag{9}$$

which represent the main terms in the power series expansions of the classical nonlinear formulas [10,12] describing realistic permeabilities. Our test computations have shown that the approximation produces virtually the same results as the more complex relations.

The kinetic rate of the hydrate-formation or dissociation reaction is much higher than the rates of diffusion and convection heat and mass transfer that control the variable fields around the reaction zone. This allows us to assume, as an accurate approximation, that the reaction occurs instantaneously and is limited to an interface of zero thickness between the hydrate-free and hydrate-filled zones without kinetic limitations. The interface is defined as a surface at which pressure and temperature follow the threshold curve $P = P_{\mathrm{eq}}(T)$ of thermodynamic stability of hydrates [see (1)].

In our model, the reaction interface is a surface of solution discontinuity, at which S_h and S_w change from in to out values, and the balances of internal energy and gas mass, taking into account reaction sources, are imposed:

$$\frac{m_s L_h S_h \rho_{h0}}{\langle\kappa\rangle_s} V_n = [\nabla_n T]_{\rm io} \tag{10}$$

$$m_s \left[S_w - S_h \left(1 - \frac{\rho_{g0}}{\rho_g} \right) \right] V_n = \frac{k_0}{\eta_g} [F_g(S_w, S_h) \nabla_n P]_{\rm io}, \tag{11}$$

where L_h is the latent heat of hydrate dissociation, V_n is the component of interface velocity normal to the interface, ∇_n is the component of gradient in the same direction, and ρ_{g0} is the mass fraction of methane within hydrate in terms of volume density. Water saturation S_w on the left-hand side of (11) is taken on the bubble's side of the interface, while the right-hand side uses the notation

$$[f]_{\rm io} = f|_{\rm in} - f|_{\rm out}$$

for the jump of field f from the hydrate-filled to the hydrate-free side of the interface.

Pressure and temperature are continuous at the interface and satisfy the equilibrium threshold (1):

$$T_{\rm in} = T_{\rm out}, \quad P_{\rm in} = P_{\rm out} = P_{\rm eq}(T_{\rm in}). \tag{12}$$

The solution is assumed to be spherically symmetric with all the variables being functions of r and t.

In the numerical analysis of Sec. IV, the governing equations are transformed into a system for gas density ρ_g, temperature T, and pressure P as variables. The system is presented in Appendix A. A finite-difference discretization of second order in space and first order in time on a uniform grid is applied. The time integration is based on an implicit scheme with sequential linearization (see, e.g., [13], [14], or [15]).

The interface balance conditions (10) and (11) are implemented using the isotherm migration method [13,14,16] adapted to a multivariable problem. In this method, additional source terms localized to the interface are added to the governing equations to reproduce the effects of heat and mass generation caused by phase transition. The method implies numerical diffusion of the interface, with the interface thickness as an adjustable parameter. In our solution, the parameter was chosen in the course of test calculations so that it provided the best agreement with the analytical solution of the Stefan problem for a plane solidification front at the same physical parameters. The resulting diffused interface thickness was between two and three grid steps.

We note that the numerical model has been developed so that it can be applied to a simulation of the arbitrary three-dimensional evolution of the system with a deformable interface. In this study, the analysis is limited to the one-dimensional (1D) spherically symmetric case. The problem is solved in the domain of radius $R_d = 4.0$ m with zero r-derivative of pressure at $r = 0$ and $r = R_d$ as boundary conditions (see Fig. 2). The initial bubble radius equals $R_0 = 4.0$ cm. The derivative of temperature equals zero at $r = 0$ and the external boundary.

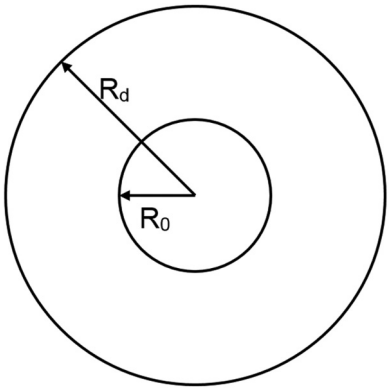

FIG. 2. Geometry of the computational model.

Grid sensitivity studies have shown that grids with $\Delta r \leqslant 0.1$ cm and $\Delta t \leqslant 100$ s produce accurate solutions.

The background temperature and pressure values (small variations of which are used for the initial state of the bubble and surrounding matrix) are $T_{\rm eq} = 280$ K and $P_0 = P_{\rm eq}(T_{\rm eq}) \approx 4.93 \times 10^6$ Pa. The other physical properties are listed in Table I. The phase saturations used in our computational study (see Sec. IV) for the systems with excess water and excess gas in the hydrate-bearing surrounding matrix are listed in Table II. The values outside and inside the bubble are connected by the relation (8) expressing mass conservation of water and a similar relation expressing mass conservation of methane.

III. ANALYTICAL SOLUTION OF THE STEFAN PROBLEM

We start by looking more closely into the nature of heat transfer in the interface area. The ratio between the rates of convection and conduction heat transfer is estimated by the Peclet number,

$$\mathrm{Pe} = \frac{UL}{\chi}, \quad \chi = \frac{\langle\kappa\rangle_s}{\langle\rho C\rangle_s}, \tag{13}$$

where L is the typical length scale, which is taken as the initial radius of the bubble $R_0 \sim 10^{-2}$ m, χ is the temperature diffusivity outside the bubble, and the typical filtration velocity U is outside the bubble. We assume the pressure equals $P_{\rm eq}(T_{\rm eq}) + \Delta P$ outside and $P_{\rm eq}(T_{\rm eq}) - \Delta P$ inside the bubble at the initial moment. The velocity U is evaluated on the basis of the Darcy resistance law [10] with the initial pressure change across the interface taken as the typical pressure variation:

$$U \sim \frac{k_0}{\eta} f(S) \frac{2\Delta P}{R_0}. \tag{14}$$

Substituting parameters from Tables I and II and assuming ΔP of the order of $10^{-4} P_{\rm eq}(T_{\rm eq})$, we find that $\mathrm{Pe} \sim 10^{-2}$ in the case of excess water and $\sim 10^{-1}$ in the case of excess gas.

TABLE II. Phase saturations outside and inside the bubble used in the numerical model.

System type	$S_{h,\rm out}$	$S_{w,\rm out}$	$S_{g,\rm out}$	$S_{h,\rm in}$	$S_{w,\rm in}$	$S_{g,\rm in}$
Excess water	0.10	0.90	0.00	0.00	0.96	0.04
Excess gas	0.50	0.00	0.50	0.00	0.39	0.61

We conclude that the convection heat transfer must be much weaker than the conduction heat transfer. This is confirmed by direct evaluation of heat transfer rates in our numerical solution of the full problem.

We see that, as an approximation that is reasonably accurate for small bubble sizes and the physical parameters considered here, we can neglect convection heat transfer and reduce the problem to that of interfacial phase change controlled by purely conduction heat transfer, i.e., the Stefan problem. In the spherically symmetric case, the governing equations and boundary conditions at the interface can be rewritten in terms of temperature deviation from the equilibrium value at the interface $\theta = T - T_{\rm eq}$:

$$\frac{\partial\theta}{\partial t} = \chi \frac{1}{r^2}\frac{\partial}{\partial r}\left(r^2\frac{\partial\theta}{\partial r}\right), \tag{15}$$

$$r \to 0, \quad \infty : \frac{\partial\theta}{\partial r} = 0, \tag{16}$$

$$r = R(t) : \theta = 0, \quad \alpha\frac{dR(t)}{dt} = \left[\frac{\partial\theta}{\partial r}\right]_{\rm oi}, \tag{17}$$

where

$$\chi = \frac{\langle\kappa\rangle_s}{\langle\rho C\rangle_s} \quad \text{and} \quad \alpha = \frac{m_s\rho_h S_h L_h}{\langle\kappa\rangle_s} \tag{18}$$

and $R(t)$ is the instantaneous location of the interface.

In the approximation, pressure variations and physical properties related to gas and water filtration become irrelevant. The difference between the excess gas and excess water cases lies solely in the values of α due to different values of hydrate saturation S_h. In the rest of this section, the analysis is conducted in terms of α and χ varying within physically possible ranges.

Our literature search has not produced a ready analytical solution of (15)–(17). It appears that the classical Stefan problem of spherically symmetric solidification or melting, while simple at first glance, is yet to obtain a complete analytical solution [17]. Solutions based on approximations or addressing special cases are, however, available. Many such solutions use expansions into power series of a small parameter, usually the reciprocal Stefan number [18–20]. Only the first several terms of such series can be evaluated analytically. The rest requires numerical solution. Another possibility is to assume an infinite solution domain and use a self-similar solution [13], possibly with two self-similar variables and in combination with a series expansion describing the initial stages of the system's evolution [21]. A review of these and other approaches can be found in [17].

We have derived a self-similar solution of the problem (15)–(17) that is valid in the case of an infinitely large domain and equilibrium initial state within the bubble. The classical self-similarity ansatz

$$\theta = f(\zeta), \quad \zeta = rt^{-1/2} \tag{19}$$

is not helpful in the case of a contracting bubble, since the resulting expression for the bubble radius $R(t) = \Gamma t^{1/2}$, where Γ is the value of ζ such that $f(\Gamma) = 0$ [see (17)], can only be used for an expanding bubble. We introduce a different ansatz based on the shifted negative time $\tau = t - t_m$ that varies from $-t_m$ to 0, where t_m is the lifetime of the bubble. The self-similarity variable becomes

$$\zeta = r|\tau|^{-1/2}. \tag{20}$$

Substitution of $\theta = f(\zeta)$ into (15) results in the ordinary differential equation

$$-\frac{1}{2\chi}\zeta f' = f'' + \frac{2}{\zeta}f'. \tag{21}$$

The interface is defined by the condition

$$\theta = f(\zeta_{\rm int}) = 0. \tag{22}$$

In accordance with (20) and following the indications produced by the numerical solution of the full problem (see Sec. IV), we take

$$\zeta_{\rm int} = \Gamma, \quad \Gamma > 0, \tag{23}$$

so the bubble radius follows:

$$R(t) = \Gamma|\tau|^{1/2}. \tag{24}$$

The energy balance condition at the interface becomes

$$-\tfrac{1}{2}\alpha\Gamma = f'_{\rm out} - f'_{\rm in}{\rm at}\zeta = \zeta_{\rm int}. \tag{25}$$

The boundary conditions at $r \to 0$ and $r \to \infty$ transform to

$$\zeta \to 0 : f' = 0, \tag{26}$$

$$\zeta \to +\infty : f' = 0. \tag{27}$$

The general solution of (21) is

$$f(\zeta) = C_2 + C_1\left(\frac{\exp(-\zeta^2/4\chi)}{\zeta} + \sqrt{\frac{\pi}{4\chi}}{\rm erf}\frac{\zeta}{\sqrt{4\chi}}\right), \tag{28}$$

$$f'(\zeta) = -\frac{C_1}{\zeta^2}\exp(-\zeta^2/4\chi), \tag{29}$$

where C_1 and C_2 are the integration constants to be determined from the boundary conditions.

Inside the bubble, (26) and (22) give $C_1 = C_2 = 0$, making (28) identically zero: $f_{\rm in} \equiv 0$. We see that the self-similar solution is only possible for the special case when the temperature inside the bubble is identically equal to the equilibrium interface temperature $T_{\rm eq}$. This limitation is not as severe as it may seem at first glance. The results of the numerical analysis discussed in the next section show that a solution starting with arbitrary slightly nonequilibrium initial conditions adjusts itself quickly so that thermodynamic equilibrium corresponding to $f_{\rm in} \equiv 0$ is established within the bubble.

Outside the bubble, the problem is underdefined, since the condition (27) is satisfied by the solution (28) and (29) automatically at any C_1 and C_2. To regularize the problem, we introduce an additional boundary condition, according to which the difference between the ambient and interface temperature tends to a constant at $r \to \infty$:

$$f_{\rm out} \to \Psi = T_{\rm out} - T_{\rm eq} < 0 \quad \text{at} \quad \zeta \to +\infty. \tag{30}$$

The value of Ψ determines the closeness of the hydrates in the surrounding matrix to instability.

The integration constants can now be expressed as

$$C_{1,\text{out}} = \frac{1}{2}\alpha\Gamma^3 \exp(\Gamma^2/4\chi), \tag{31}$$

$$C_{2,\text{out}} = \Psi - \frac{1}{2}\sqrt{\frac{\pi}{4\chi}}\alpha\Gamma^3 \exp(\Gamma^2/4\chi). \tag{32}$$

The boundary condition (27) leads to the transcendental equation for Γ:

$$\Psi + \frac{1}{2}\sqrt{\frac{\pi}{4\chi}}\alpha\Gamma^3 \exp(\Gamma^2/4\chi)\left(\text{erf}\frac{\Gamma}{\sqrt{4\chi}} - 1\right) + \frac{1}{2}\alpha\Gamma^2 = 0. \tag{33}$$

Introducing $y = \Gamma/\sqrt{4\chi}$, we can rewrite the equation in a compact form:

$$\frac{\Psi}{2\chi\alpha} = y^2[\sqrt{\pi}\, y \exp(y^2)(1 - \text{erf}\, y) - 1]. \tag{34}$$

The equation can be solved numerically. Typically, it has two solutions, one with negative and one with positive Γ. Only the second solution is, evidently, physically relevant.

The evolution of the bubble radius (24) can be rewritten in physical variables as

$$R(t) = R_0\left(1 - \frac{t}{t_m}\right)^{1/2}, \tag{35}$$

$$\frac{dR(t)}{dt} = -\frac{1}{2}\frac{R_0}{t_m^{1/2}}\left(1 - \frac{t}{t_m}\right)^{-1/2}, \tag{36}$$

where the initial radius R_0, lifetime t_m, and constant Γ are related as

$$\Gamma \sim \frac{R_0}{t_m^{1/2}}. \tag{37}$$

We have computed roots of (34) in a broad range of parameters. The results are presented in Fig. 3. In the framework of our model neglecting the convection heat transfer, the sole difference between the two cases is, evidently, in the value of the hydrate saturation $S_{h,\text{out}}$, which affects the value of the interface coefficient α. All other parameters being equal, higher saturation in the excess gas case means lower Γ and longer lifetime (see Fig. 3). As an example, for a bubble of initial radius 4 cm at $\Psi = -10^{-2}$ K, our results show $t_m \approx 5.8 \times 10^5$ s in the case of excess water and $t_m \approx 3.0 \times 10^6$ s in the case of excess gas.

The solution shown in Fig. 3 demonstrates that Γ and, thus, the lifetime of a bubble of a given radius are strongly affected by α and the temperature difference Ψ, but not by the thermal diffusivity χ. The solution can be compared with the qualitative estimate of freezing time obtained for the classical spherical Stefan problem [21]. In the limit of large inverse Stefan number determined as

$$\text{Ste}^{-1} = -\frac{m_s S_h L_h}{\langle\rho C\rangle_s \Psi} \tag{38}$$

($\text{Ste}^{-1} \sim 10^3$–$10^4$ in our system), the estimate corrected to take into account the volume content of hydrate is

$$t_m^* \sim -\frac{R_*^2 m_s S_h \rho_h L_h}{\langle\kappa\rangle_s \Psi}\tau_e = -\frac{R_*^2}{\Psi}\tau_e\alpha, \tag{39}$$

where $R_* = 2/3R_0$ is the time-averaged radius of the bubble and τ_e is a constant approximately equal to 1 [21]. Our results are in good agreement with (39). For example, the lifetimes of a bubble of initial radius 4 cm reported above are close to the estimates by (39): 5.3×10^5 s in the case of excess water and 2.7×10^6 s in the case of excess gas.

IV. NUMERICAL SOLUTION OF THE FULL PROBLEM

The numerical simulation is provided for system parameters shown in Table I with phase saturations in the excess gas and excess water cases listed in Table II.

Two kinds of initial conditions are used. The first is employed to reproduce the self-similar solution (28) numerically using the full system (3)–(7) including the fluid flows and convective heat transfer. The initial pressure is constant P_{eq} throughout the computational domain, while the temperature

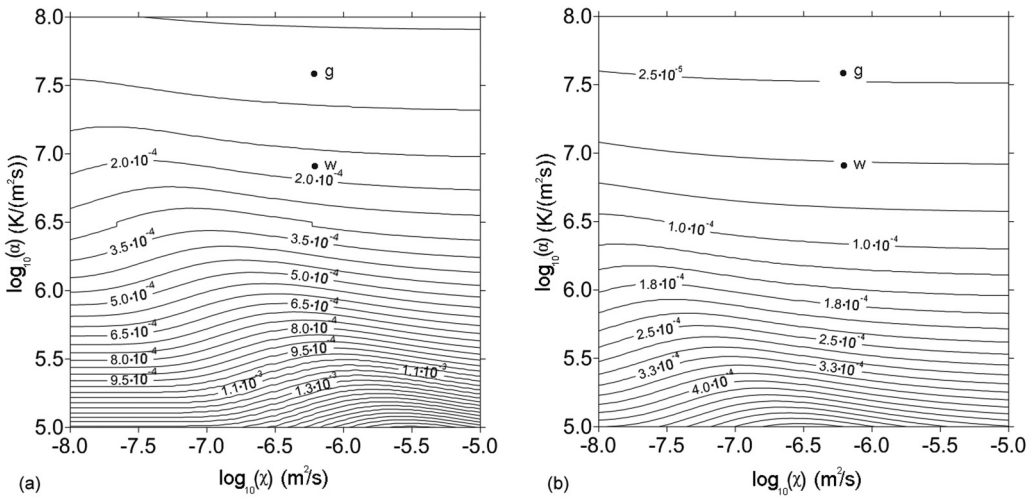

FIG. 3. Results of the analytical solution. Constant Γ [see (37)] is shown as a function of thermal diffusivity χ and interface parameter α [see (18)] for the difference between the far-field ambient and interface temperature Ψ equal to -10^{-1} K (a) and -10^{-2} K (b). Points marked by indices g and w indicate the systems with excess gas and excess water considered in the numerical analysis of Sec. IV.

distribution initially follows the self-similar solution (28) with constants C_1 and C_2 determined from (31) and (32):

$$\theta(r) = 0 \quad \text{at} \quad r \leqslant R_0, \tag{40}$$

$$\theta(r) = \Psi + \frac{1}{2}\alpha\Gamma^3\frac{\sqrt{t_m}}{r}\exp\left[\left(\Gamma^2 - \frac{r^2}{t_m}\right)\Big/4\chi\right] + \frac{1}{2}\frac{\pi}{4\chi}\alpha\Gamma^3\exp(\Gamma^2/4\chi)[\mathrm{erf}(r/\sqrt{4\chi t_m}) - 1]$$

$$\text{at} \quad r > R_0, \tag{41}$$

where Γ and t_m are obtained from (34). The initial value of temperature at the outer boundary of computational domain $r = R_d$ corresponds to $T_{\text{out}} = T_{\text{eq}} + \Psi$ [see (30)].

To verify the numerical method and the analytical solution of Sec. III, computations are first conducted with the gas and water velocities set to zero. The computed and analytical results are found to be in nearly perfect agreement with each other. A small (within a few percent) difference between the temperature profiles is observed far from the bubble, which can be attributed to the numerical discretization error of the scheme. The computed radius of the bubble follows the analytical solution very closely.

The numerical solution of the full system of equations is compared with the analytical solution in Figs. 4(a) and 4(b). We see that the bubble radius (marked as a point where θ first deviates from zero) evolves in good quantitative agreement with the analytical solution. Comparing the temperature profiles, we see very good agreement in the case of excess gas [see Fig. 4(b)]. On the contrary, the temperature profiles computed in the case of excess water show significant deviation from the analytical solution. This can be attributed to the effect of convection heat transfer by water just outside the interface. We conclude that this effect is important and should be taken into account if realistic distributions of temperature are desired.

In the second set of simulations, we investigated the effect of various types of nonequilibrium initial conditions. In particular, pressure was initially set to $P = P_{\text{eq}}(T_{\text{eq}}) + \Delta P$ outside the bubble and $P = P_{\text{eq}}(T_{\text{eq}}) - \Delta P$ inside it. Here, $\Delta P = 10^{-4} P_{\text{eq}}$ was a small excess pressure, which set the system's closeness to thermodynamic instability. The temperature was initially constant, $T_{\text{eq}} - \Psi$, outside the bubble. Inside, the temperature was either T_{eq} or increased according to

$$T - T_{\text{eq}} = A\{\exp[-a(r/R_0)^2] - \exp(-a)\}, \tag{42}$$

where the constants were $A = 3$ K and $a = -0.016$ selected so that the maximum temperature increase within the bubble was about 0.05 K.

The main result was that the nonequilibrium initial states only affected the early stages of the bubble evolution. The pressure adjusted to a uniform constant value in the entire domain. This was accompanied by a jumplike reduction of the bubble radius. Temperature became uniform inside the bubble and corresponded approximately to the analytical solution outside it. The time scale of temperature adjustment was larger than that of pressure adjustment but still much smaller than the total lifetime of the bubble, t_m.

After the initial adjustment, the computed solution followed the analytical solution with small deviation due to the convection effects and numerical discretization error. Most importantly, the bubble radius evolved in accordance with the square-root law given by (35). The computed lifetime t_m as a function of the system's physical parameters was in good agreement with the values of Γ [see (37)] predicted by the analytical solution, with the difference being first not large and second fully accounted for by the initial adjustment. We can conclude that the analytical solution of Sec. III gives an accurate prediction of the bubble lifetime in the conditions considered in this paper.

V. IMPLICATIONS FOR THE DYNAMICS OF HYDRATE-BEARING SEDIMENTS

We can now return to the main motivation of our study stated in the introductory section of this paper, namely to the role of the typical lifetime of bubbles in the dynamics of hydrate-saturated deposits. We start with the possibility of the

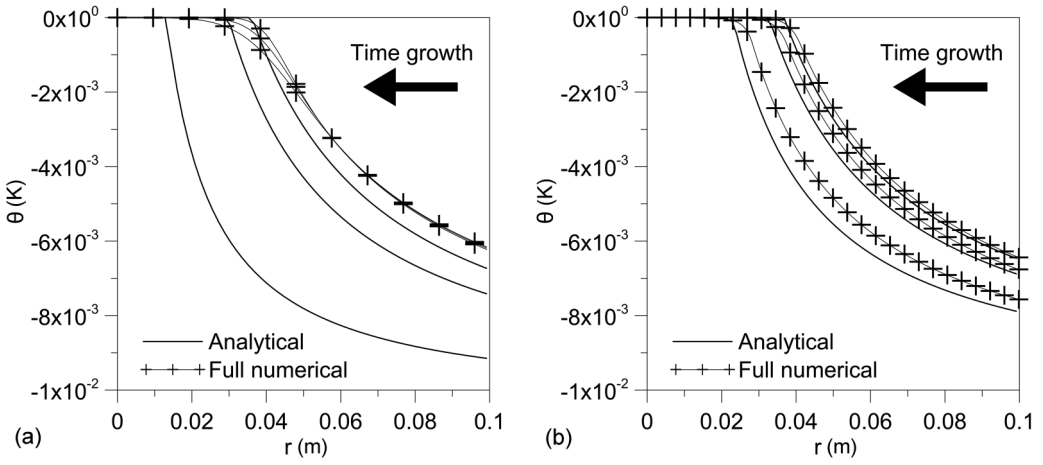

FIG. 4. Comparison between the analytical self-similar solution and the numerical solutions of the full problem with initial conditions taken from the self-similar solution (40) and (41). Temperature distributions for three moments of time are shown at $\Psi = -0.01$ K for the cases of excess water (a) and gas (b).

transport of methane to the surface by floating-up bubbles. Here, a direct assessment can be made assuming that the hydrate layer has excess water and that the filtration is driven by the buoyancy force. The velocity of a bubble's upward motion can be estimated as in [22]:

$$V = \frac{2k_0 g(\rho_i - \rho_o)}{m_s(2\eta_i + \eta_o)}, \tag{43}$$

where ρ, η are the effective density and viscosity of fluid inside and outside the bubble. Using the system properties listed in Tables I and II, we find that a bubble has velocity of the order of 10^{-8} m/s. The results of the analytical solution summarized in Fig. 3 show that under physically possible conditions, the value of Γ is never smaller than 10^{-6}, a more likely value being about 10^{-5}. Taking $\Gamma = 10^{-6}$ and considering bubbles of initial radii less than 10 cm, we obtain the upper limit estimate of the bubble lifetime as $t_m \sim 10^8$ s. This means that the bubble passes a distance less than 1 m over its lifetime, which is, of course, much smaller than the typical thickness of the hydrate stability zone. We conclude that no such bubbles, unless they are generated very close to the upper surface of the hydrate layer, can survive long enough to deliver methane directly to the atmosphere.

At the same time, at a high concentration of bubbles, the contribution of their motion into cumulative gas transport can be significant in comparison to transport by diffusion. This means that the commonly used diffusion-based assessments of the gas filtration rate have to be reconsidered in situations in which the existence of hydrate-free bubbles is suspected. The list of such situations may include, for example, the surroundings of an extraction well or the surroundings of the often observed excursions of free methane gas into the hydrate-bearing zone arising due to variations of local properties of the deposits (see, e.g., [8]).

The existence of hydrate-free bubbles increases the average permeability of a porous medium. Even if the effect is limited in time, it may have significant implications for the dynamics of the hydrate-bearing deposits. In particular, it leads to stronger flows of water and gas, and it may facilitate instabilities of the system. One example of such instability occurring at the lower boundary of the hydrate layer separating it from the underlying layer saturated with free methane gas has been presented in [23]. Other instabilities, including those occurring inside the hydrate-bearing layer and leading to the development of large areas with dissociated hydrates or chimney-like hydrate-free channels, are theoretically possible, but they require both observational and modeling studies. Whether a bubble with an expected lifetime of the order $t_m \sim 10^8$ plays a role in such instabilities remains to be seen.

VI. CONCLUDING REMARKS

We have studied the evolution of a small (a few cm) hydrate-free inclusion within the hydrate bearing sediments. The problem has been solved numerically in the framework of a full model describing the phase transition and heat and mass transport and analytically using the model, in which flows of gas and water are neglected. In the case of the simplified model, the problem can be set as a Stefan problem, for which we have found a self-similar solution. According to the solution, the radius of the bubble follows the square root law by (35) and its lifetime is determined by (37) with the parameter Γ being primarily a function of the interface parameter α [see (18)]. The role of the second parameter χ expressing the thermal diffusivity is significantly smaller.

From the comparison between the numerical and analytical solutions, we have found that the evolution of the bubble's radius and its lifetime are accurately represented by the simplified model. At the same time, the difference between the temperature profiles found in the two solutions indicates that the convection heat transfer, especially that produced by water flow, should be taken into account if an accurate representation of heat transfer properties is desired. This is particularly true in problems with multiple bubbles, where their concentration is high enough to affect the state of the surrounding deposits.

An important result of our study is an estimate of the typical lifetime of a bubble. It has been found that the lifetime is usually too short for the bubble to reach the upper surface of the hydrate layer. At the same time, the lifetime is not negligibly small, which means that the presence of bubbles in the hydrate-saturated layer can make a significant contribution to the heat and mass transport through the layer. The presence of the bubbles increases volume-averaged relative permeability and may significantly affect the dynamics of hydrate-bearing sediments in response to an extraction well or the increase of surface temperature.

The results obtained in this paper do not apply to the case of large bubbles, when the assumptions of negligible inertia and convection transport become invalid. In that case, one has to consider instabilities and deformation of the bubble surface, and the predictions of lifetime and filtration speed have to be reconsidered. The self-similar solution obtained in this paper can be used as an initial point for such studies, where the presence of convection heat and mass transfer, the geothermal gradient, can be taken into account.

ACKNOWLEDGMENTS

Work was financially supported by the Civilian Research and Development Foundation (Grant No. RUP1-2945-PE-09) and the Russian Foundation for Basic Research (Grant No. 09-01-92505).

APPENDIX: TRANSFORMED EQUATIONS

For the numerical solution, the governing equations (3)–(7) are transformed by direct substitution of the velocities into the heat and mass conservation equations. In this way, we obtain the system of three equations for the pressure P, temperature T, and gas density ρ_g. The phase saturations are assumed constant inside and outside the bubble.

The transformed system of equations is as follows:

$$m_s\,(1 - S_h - S_w)\,\frac{\partial \rho_g}{\partial t} = \frac{k_0}{\eta_g} F_g(S_g, S_w)(\rho_g \nabla^2 P + \nabla \rho_g \cdot \nabla P), \tag{A1}$$

$$\langle \rho C \rangle_s \frac{\partial T}{\partial t} = \langle \kappa \rangle_s \nabla^2 T + k_0 \left(\frac{\rho_g C_g F_g(S_g, S_w)}{\eta_g} + \frac{\rho_w C_w F_w(S_g, S_w)}{\eta_w} \right) \nabla P \cdot \nabla T, \quad \text{(A2)}$$

$$P = \rho_g R T, \quad \text{(A3)}$$

where the notation is as in Sec. II.

Analyzing the computed solutions, we have found that there are always two stages of the time evolution of the system. The first is the rapid adjustment from the initial conditions to the state resembling the analytical solution of Sec. III with equilibrium inside the bubble. The second stage is the slow evolution with the bubble's radius following the self-similar formula (35). During this stage, the gas density ρ_g is nearly constant in the entire solution domain. According to (A1), this implies $\nabla^2 P = 0$, i.e., the water velocity satisfying the incompressibility condition $\nabla \cdot \boldsymbol{v}_w = \mathbf{0}$. This confirms, *a posteriori*, the validity of our assumption of constant water saturation S_w. We note that the situation that was just described is only realized in the case of small bubbles considered in this paper. Our preliminary simulations of large (about 0.5 m) deformable inclusions show that the variations of S_w are not negligible, and the equation-of-mass conservation of water has to be added to (3)–(7).

[1] Y. Makogon, *Hydrates of Hydrocarbons* (Pennwell, Tulsa, Oklahoma, 1997).

[2] E. Sloan and C. Koh, *Clathrate Hydrates of Natural Gases* (CRC, Boca Raton, FL, 2008).

[3] B. Buffet and D. Archer, Earth Planet. Sci. Lett. **227**, 185 (2004).

[4] D. Archer, Biogeosciences **4**, 521 (2007).

[5] J. Kennett, K. Cannariato, I. Hendy, and R. Behl, *Methane Hydrates in Quaternary Climate Change: The Clathrate Gun Hypothesis* (American Geophysical Union, Washington, DC, 2003).

[6] W. Xu and R. Lowell, Geophys. Res. **106**, 26413 (2001).

[7] N. Shakhova and I. Semiletov, J. Marine Sys. **66**, 227 (2007).

[8] X. Liu and P. Flemings, Earth Planet. Sci. Lett. **241**, 211 (2006).

[9] G. Moridis, SPE J. **8**, 359 (2003).

[10] D. Nield and A. Bejan, *Convection in Porous Media*, 4th ed. (Springer, New York, 2013).

[11] G. Tsypkin, Ann. N.Y. Acad. Sci. **912**, 428 (2000).

[12] G. Moridis, M. Kowalsky, and K. Pruess, *TOUGH + Hydrate v1.0 User's Manual: A Code for the Simulation of System Behavior in Hydrate-bearing Geologic Media* (Lawrence Berkeley National Laboratory, Berkeley, CA, 2008).

[13] A. Samarskii and P. Vabishchevich, *Computational Heat Transfer—Vol. 1, Mathematical Modeling* (Wiley, Chichester, 1996).

[14] A. Samarskii, *The Theory of Difference Schemes* (Dekker, New York, 2001).

[15] O. Zikanov, *Essential Computational Fluid Dynamics* (Wiley, Hoboken, NJ, 2010).

[16] J. Crank and R. Gupta, Int. J. Heat Mass Transf. **18**, 1101 (1975).

[17] S. McCue, B. Wu, and J. Hill, Proc. R. Soc. A **464**, 2055 (2008).

[18] R. Pedroso and G. Domoto, J. Heat Transf. **95**, 42 (1973).

[19] D. Riley, F. Smith, and G. Poots, Int. J. Heat Mass Transf. **17**, 1507 (1974).

[20] K. Stewartson and R. Waechter, Proc. R. Soc. A **348**, 415 (1976).

[21] A. Soward, Proc. R. Soc. A **373**, 131 (1980).

[22] D. Lyubimov, S. Shklyaev, T. Lyubimova, and O. Zikanov, Phys. Fluids **21**, 014105 (2009).

[23] E. Kolchanova, T. Lyubimova, D. Lyubimov, and O. Zikanov, Theor. Comput. Fluid Dyn. **27**, 637 (2013).